ACS APPLIED MATERIALS & INTERFACES

Research Article

www.acsami.org

Enhanced Hole Carrier Transport Due to Increased Intermolecular Contacts in Small Molecule Based Field Effect Transistors

Satej S. Dharmapurikar,[†,‡] Arulraj Arulkashmir,[†,‡] Chayanika Das,[†,‡] Pooja Muddellu,[†] and Kothandam Krishnamoorthy*[,†,‡,§]

[†]Polymer Science and Engineering Division, CSIR-National Chemical Laboratory, Pune 411008, Maharashtra, India

[‡]Academy of Scientific and Innovative Research, New Delhi, India

[§]CSIR-Network Institute of Solar Energy, New Delhi, India

Supporting Information

ABSTRACT: Small molecules and oligomers can be synthesized with very high purity and precise molecular weights, but they often do not form uniform thin films while processed from solution. Decreased intermolecular contacts between the small molecules are another disadvantage. To increase the intermolecular contacts in small molecules, we have chosen *i*-indigo, as one of the conjugated molecular units. The electron poor *i*-indigo has been connected with electron rich triphenylamine to synthesize a donor−acceptor−donor type small molecule. The propeller shaped triphenylamine helps to increase the solubility of the small molecule as well as isotropic charge transport. The intermolecular spacing between the molecules has been found to be low and did not vary as a function of thermal annealing. This implies that the intermolecular contacts between the small molecules are enhanced, and they do not vary as a function of thermal annealing. Organic field effect transistors (OFET) fabricated using a small molecule exhibited a hole carrier mobility (μ) of 0.3 $cm^2/(V\ s)$ before thermal annealing. A marginal increase in μ was observed upon thermal annealing at 150 °C, which has been attributed to changes in thin film morphology. The morphology of the thin films plays an important role in charge transport in addition to the intermolecular spacing that can be modulated with a judicious choice of the conjugated molecular unit.

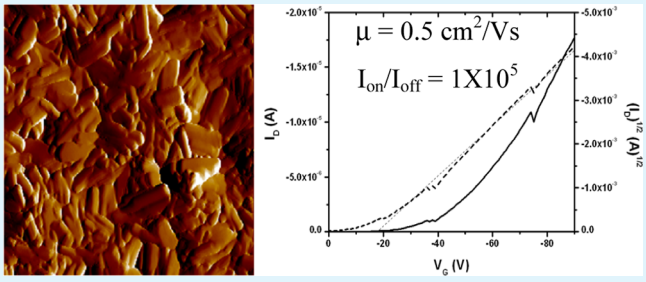

KEYWORDS: *small molecules, i-indigo, triphenylamine, organic field effect transistor, quadrupole interaction, hole mobility*

1. INTRODUCTION

Conjugated polymers (CPs) have become the material of choice for the fabrication of organic electronic devices due to easy processability, controllable band gap, and good charge transport properties.[1−6] CPs do suffer from device inconsistencies arising from batch-to-batch variations, polydispersity, and end group contaminations. On the other hand, small molecules and oligomers can be synthesized with precise molecular weight and high purity that eliminates material inhomogeneities.[7−9] Small molecules often do not form films; hence the devices are prepared by thermal evaporation.[8] If this issue is circumvented, small molecules will have the combination of advantages of the polymers and small molecules. To solution process small molecules, various approaches have been developed.[10−13] In these systems, the chain to chain contacts are limited that adversely impact the device efficiency. To improve the contact between chains, small molecules with π stacking functionalities have been prepared. The devices prepared with small molecules comprising π stacking functionalities show better efficiency than the ones without them.[14] Recently, quadrupole−quadrupole interactions between lactum containing diketopyrrolopyrrole small molecules have been shown to favor intermolecular contacts.[15] We hypothesized that such interaction is possible in the *i*-indigo containing small molecules.

CPs with electron deficient units have been prepared to increase the ionization potential and impart air stability.[3] Incorporation of electron deficient units into an electron rich conjugated backbone is widely mentioned as the Donor−Acceptor−Donor (D−A−D) system.[16−24] These polymers show high charge carrier mobility despite having less ordered microstructures.[3,25] Thus, a processable D−A−D small molecule is an attractive candidate because it encompasses the advantages of polymers and small molecules. *i*Ind is an electron deficient molecule with a lactam ring,[3,16,26−28] which has been explored for the synthesis of polymers with μ ranging from 1×10^{-3} to 2.4 $cm^2/(V\ s)$.[26−28] The lower μ was observed while using weak donors with *i*Ind that leads to poor intermolecular contacts despite the presence of a lactam ring, which was hypothesized to make better intermolecular

Received: April 16, 2013
Accepted: June 28, 2013
Published: June 28, 2013

Scheme 1. Synthesis of Small Molecules 4a−d

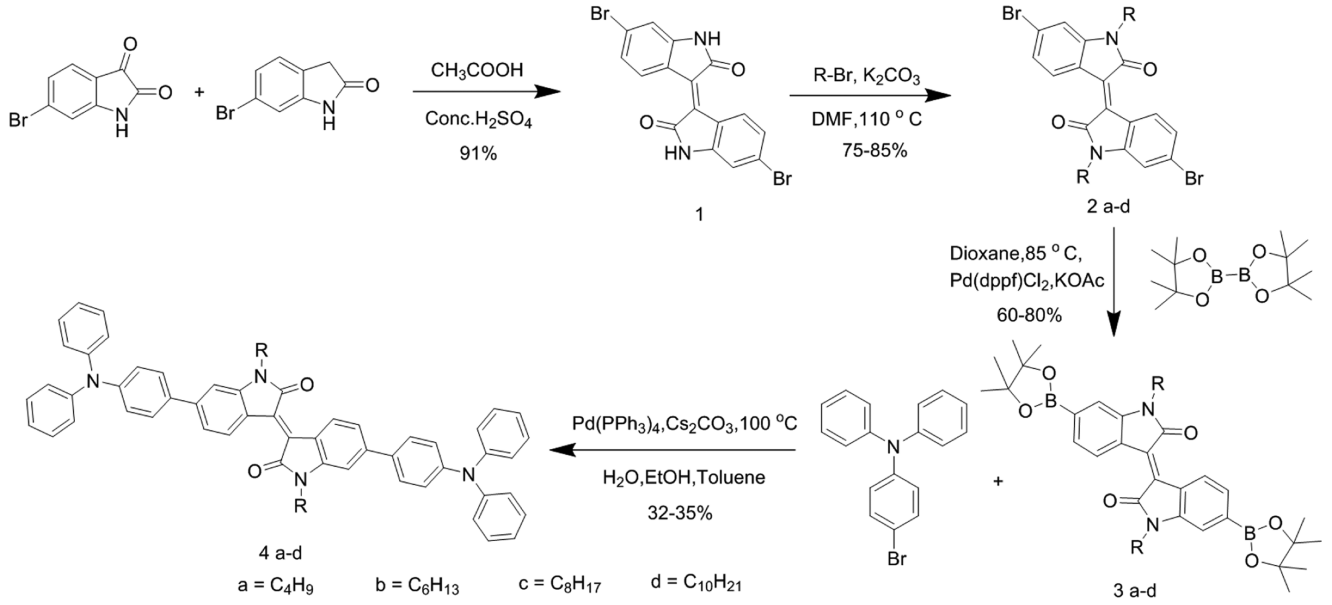

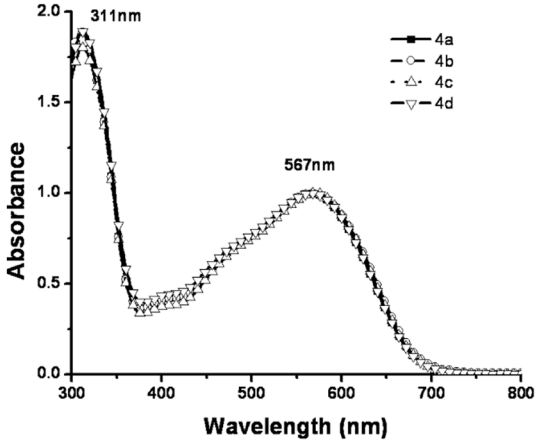

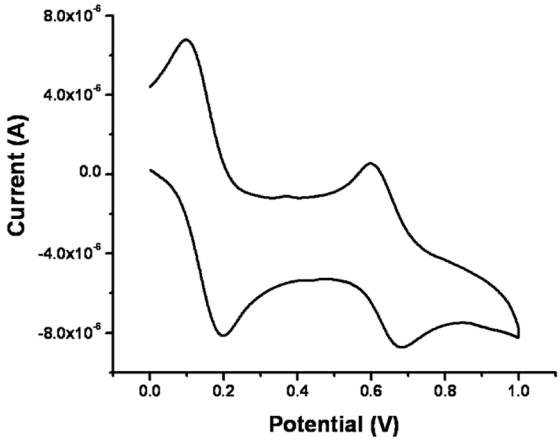

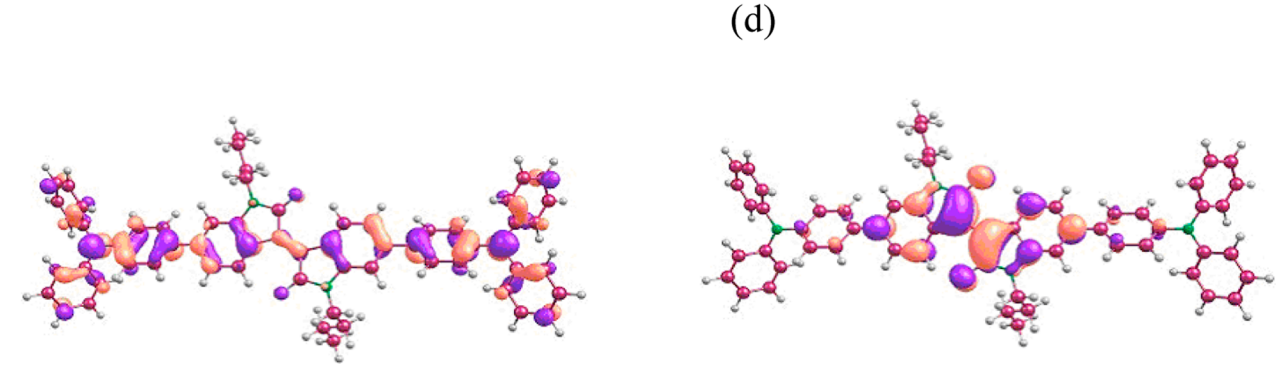

Figure 1. UV−vis absorption spectra of **4a−d** in $CHCl_3$ (a) and cyclic voltammogram of **4a** with ferrocene as internal standard (b). HOMO (c) and LUMO (d) plot for **4a**.

contact.[28] Thus, in our design, *i*Ind has been connected with triphenylamine (TPA), which is a strong donor. Furthermore, TPA comprising small molecules has been shown to form glasses with isotropic charge transport properties.[29−31] We hypothesized that the solubility of TPA containing molecules would be enhanced due to the propeller shape of the TPA

dx.doi.org/10.1021/am401379a | ACS Appl. Mater. Interfaces 2013, 5, 7086−7093

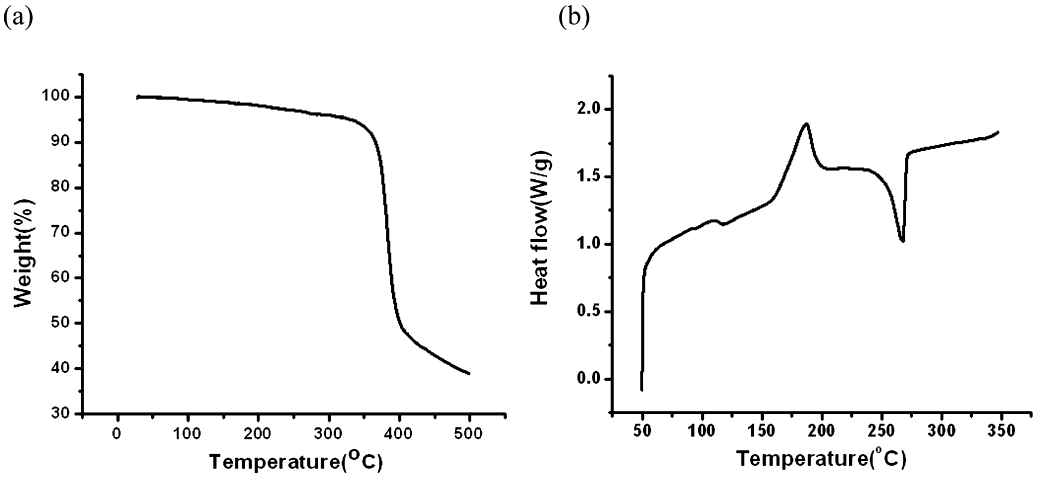

Figure 2. Thermogravimetric analysis curve (a) and differential scanning calorimetry curve (b) of **4a**.

Table 1. Electronic, Thermal, And Morphological Properties of Small Molecules

molecule	T_g (°C)	T_c (°C)	T_m (°C)	$R_a{}^a$	$R_a{}^b$	μ (cm^2/(V s))^a	V_T (V)^a	$I_{on/off}{}^a$	μ (cm^2/(V s))^b	V_T (V)^b	$I_{on/off}{}^b$
4a	105	165	266	1.0	1.2	7.3×10^{-4}	−12	0.7×10^2	1.0×10^{-3}	−7	0.4×10^3
4b	90	161	242	1.3	1.7	1.7×10^{-5}	−35	0.5×10^2	1.3×10^{-3}	−15	0.6×10^3
4c	93	167	258	1.2	1.4	0.30	−21	1×10^5	0.50	−18	1×10^5

^{a}As prepared. ^{b}After thermal annealing.

moiety. We were interested in studying the effect of the alkyl chain on the performance of the small molecules in OFET because alkyl chains do impact the charge carrier mobility due to the formation of insulating domains.[32,33] Alkyl chains have also been shown to assist the packing of the molecules.[34,35] Usually, the charge carrier mobility and device efficiency have been found to nonlinearly increase as a function of the number of carbons in the alkyl chain.[36−39] Thus, it is necessary to vary the number of carbon atoms in the alkyl chain and identify the optimum chain length. Toward this objective, we have synthesized TPA-*i*Ind-TPA small molecules with various alkyl chains, fabricated FET devices, studied the device performance, and correlated it with the film morphology.

2. RESULTS AND DISCUSSION

Synthesis of TPA-*i*Ind-TPA is shown in Scheme 1. Bromoisatin and 6-bromoindole were reacted in the presence of acid to get compound **1**.[40,41] This was then reacted with alkyl bromide to get compound **2**. Further reaction of **2** with boronic ester resulted in the formation of **3**. The targeted small molecules (**4**) were synthesized by reacting **3** with bromotriphenylamine. The molecules **4a−d** have butyl, hexyl, octyl, and decyl chains, respectively.

Absorption profiles of the small molecules (**4a−d**) in dilute chloroform solutions are shown in Figure 1a. Small molecules **4a−d** show two absorption maxima with a low energy peak at 575 nm and a high energy peak at 320 nm. A weak absorption hump at 400 nm can also be seen in these spectra. The absorption spectrum of TPA in chloroform shows a peak at 305 nm. The chloroform solution of *i*Ind alone has two absorption maxima at 400 and 500 nm. Considering these absorption maxima, the peaks at 320 and 575 nm (**4a−d**) can be assigned to TPA and *i*Ind based transitions, respectively. The 75 nm bathochromic shift observed for **4a−d** compared to *i*Ind is the result of a decrease in band gap imparted by TPA. The bathochromic shift and concurrent decrease in band gap was expected due to the formation of a molecule with alternate electron rich and electron poor moieties. From the onset of the low energy peak, the band gap was calculated to be 1.8 eV for **4a−d**. In order to determine the band edges of **4a−d**, cyclic voltammograms were recorded using 0.1 M tetrabutylammonium perchlorate as a supporting electrolyte in chloroform. Pt wire was used as a working electrode. $Ag/AgNO_3$ was used as a reference electrode, and Pt foil was used as counter electrode. The voltammograms were calibrated against the Fc/Fc^+ redox couple to determine the frontier orbital energy levels.

The potential of the working electrode was swept between 0 and 1 V. The oxidation and reduction peaks were observed at 670 mV and 570 mV, respectively (Figure 1b). The HOMO energy level was determined to be −5.3 eV using the following formula HOMO = $-(E_{ox(Fc/Fc+),onset} + 4.8)$ eV. The HOMO energy level of **4a−d** is 0.1 eV below the oxygen energy level (−5.2 eV);[42] hence they are air stable. By adding the band gap determined from the absorption spectra, the LUMO was calculated to be −3.5 eV. In the negative sweep, a clear reduction peak was observed at −1.25 V. From the onset of the reduction and oxidation peaks, the band gap was calculated to be 1.7 eV.

Density functional theory (DFT) calculations have been carried out to gain a deeper insight into the energy levels and distribution of wave functions in **4a−d**. The energy levels were calculated using the B3LYP functional and polarized 6-31g* basis set. The surface plots for **4a** are shown in Figure 1c and d. The remaining surface plots are shown in the Supporting Information (Figure S13−S15). The DFT calculation shows that the LUMO wave function of all the TPA-*i*Ind-TPA resides exclusively on the *i*Ind moiety, which is likely due to the electron accepting nature of the *i*Ind. Whereas, the wave function of the HOMO energy level is delocalized over the whole molecule; i.e., both *i*Ind and TPA have contributed to the HOMO energy level. Indeed, this is the reason for the high lying HOMO energy of −5.3 eV for TPA-*i*Ind-TPA compared

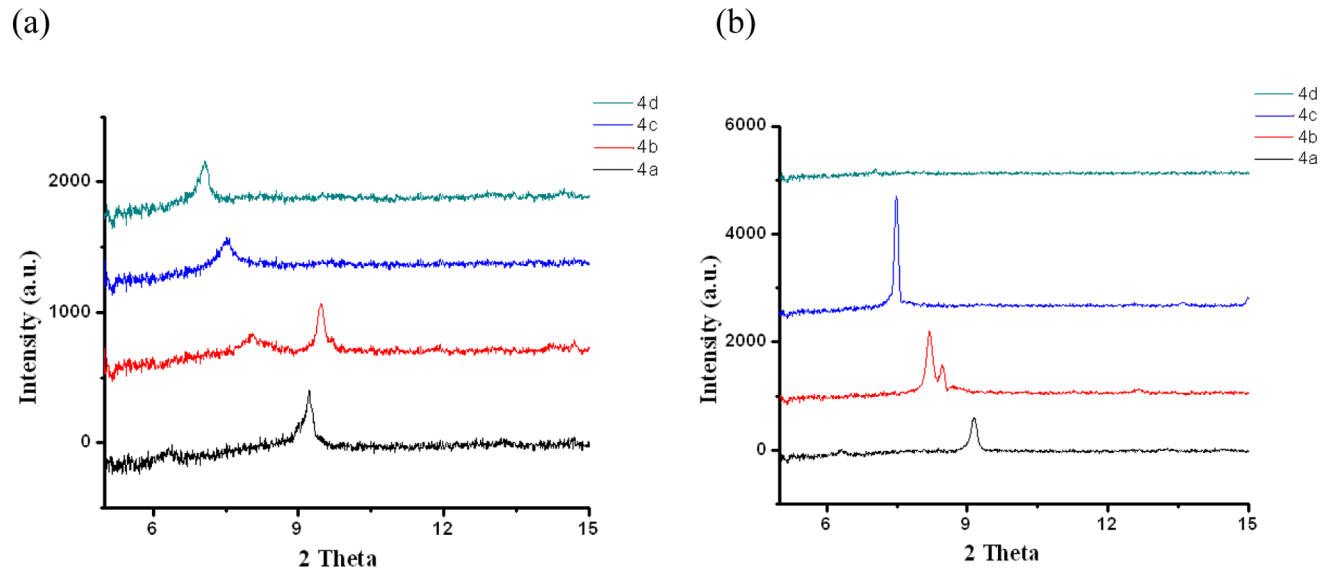

Figure 3. XRD patterns of molecules **4a–d** before thermal annealing (a) and after thermal annealing (b).

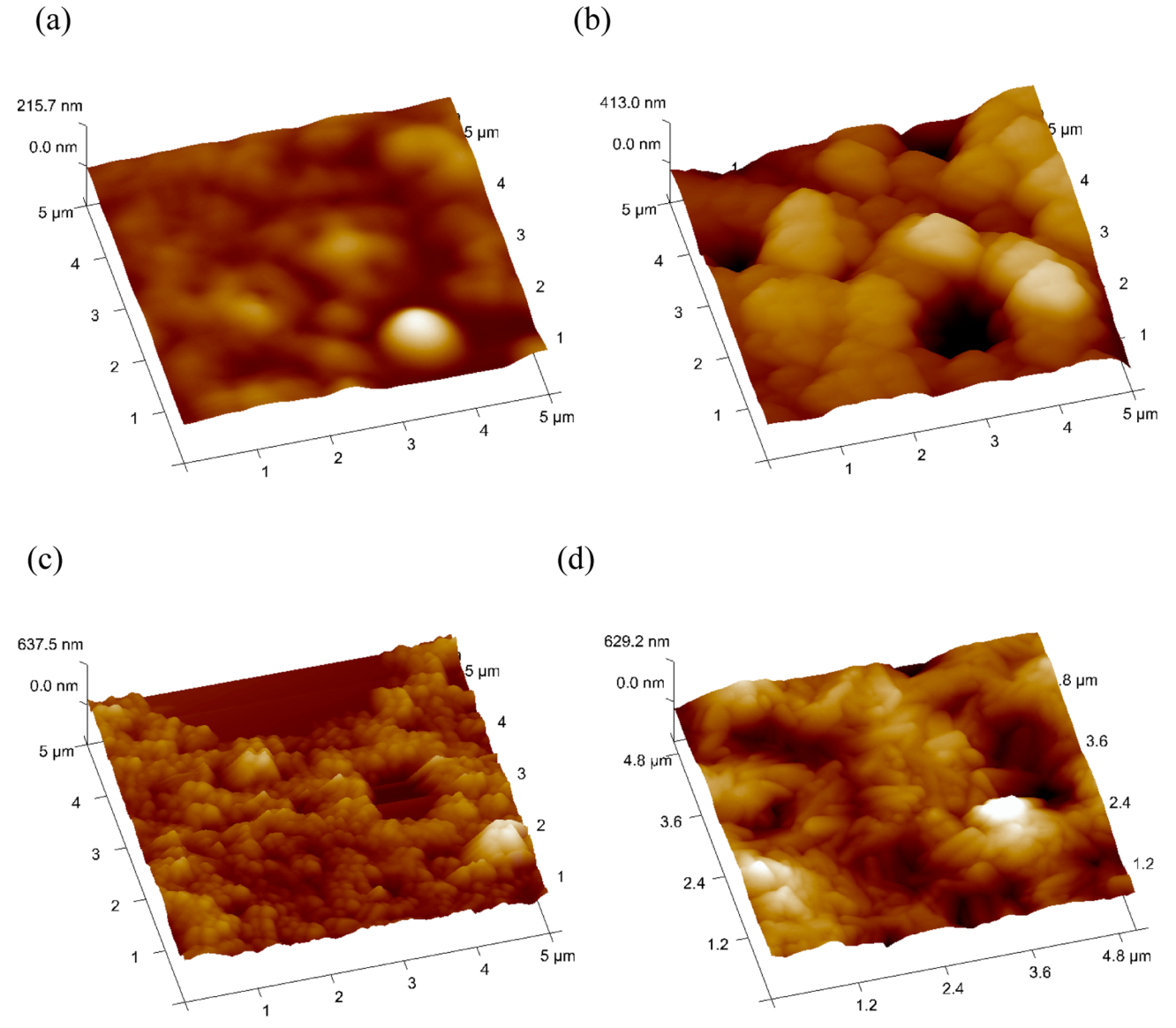

Figure 4. AFM image of thin films of unannealed **4a** (a), annealed **4a** (b), unannealed **4c** (c), and annealed **4c** (d).

dx.doi.org/10.1021/am401379a | *ACS Appl. Mater. Interfaces* 2013, 5, 7086–7093

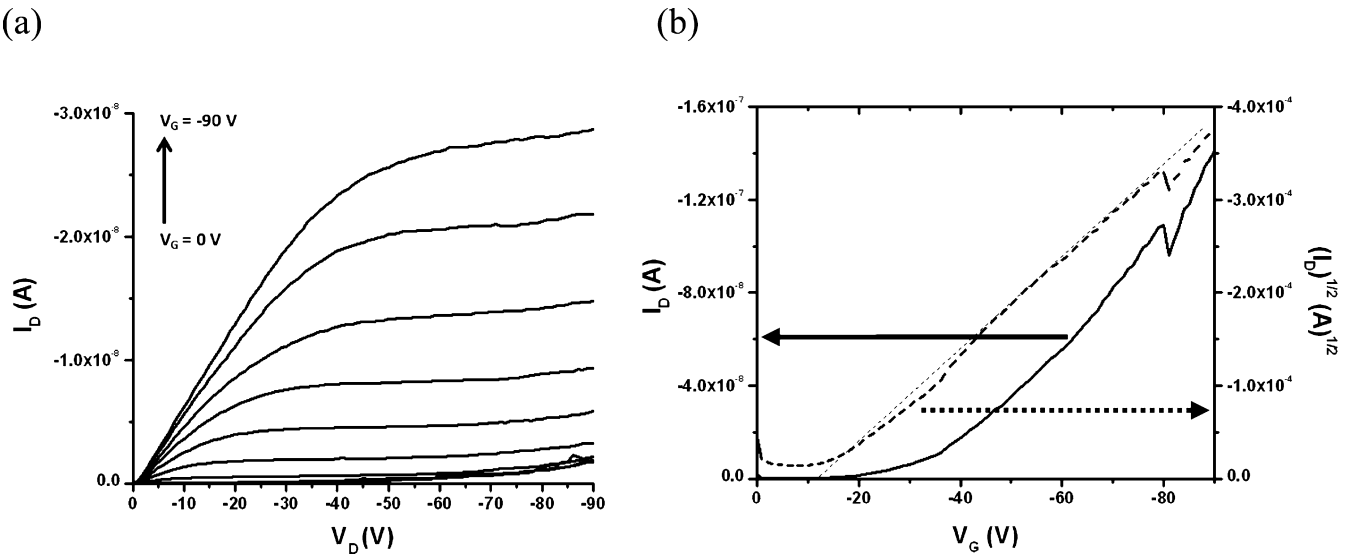

Figure 5. (a) Output characteristic curve of **4a** before thermal annealing. (b) Transfer characteristic curve of **4a** before thermal annealing.

to −5.4 eV observed for TPA alone. The thermal characteristics of **4a**−**d** were studied using TGA and DSC. All the compounds were found to be thermally stable up to 350 °C (Figure 2a). The DSC curves of **4a**−**c** show the glass transition temperature (T_g), crystallization temperature (T_c), and melting temperature (T_m), which are provided in Table 1. The T_g is highest for **4a** and decreases upon an increase in alkyl chain length (**4b** and **4c**) due to free volume between the molecules. Similarly, T_m and T_c also decrease upon an increase in alkyl chain length. A representative DSC curve is shown in Figure 2b. In the case of **4d**, no clear phase transition peaks are observed (Supporting Information Figure S29). It may be due to the close T_c and T_m temperatures.

Thin film XRD spectra were recorded to gain deeper understanding on the interplanar spacing of **4a**−**d** as a function of thermal annealing.[43,44] Thin films of the molecules showed diffraction peaks at 9.31 (**4a**), 9.2, 7.91 (**4b**), 7.51 (**4c**), and 7.04 (**4d**) in the XRD spectra recorded between 2θ of 5 and 30 (Figure 3a). No peaks were observed while the XRD spectra were recorded between 0.5 and 5 (2θ). Using the Bragg equation, the observed 2θ corresponds to a d spacing of 9.5 (**4a**), 11.1, 9.5 (**4b**), 11.7 (**4c**), and 12.6 Å (**4d**).

It is necessary to note that the d spacing observed for **4a**−**d** is significantly lower than that observed for diketopyrrolopyrrole and oligothiophene based small molecules.[43,44] The lower d spacing is an indication of decreased intermolecular distance, hence better contacts between the molecules. After thermal annealing at 150 °C (temperature used for device annealing), the XRD spectra were recorded, wherein peaks were observed at 9.31 (**4a**), 8.20, 8.32 (**4b**), 7.51 (**4c**), and 7.04 (very low intensity peak; **4d**; Figure 3b). The d spacing calculated for these 2θ were 9.5 (**4a**), 10.8, 10.4 (**4b**), 11.7 (**4c**), and 12.6 (**4d**). The thermal annealing had very little impact on the d spacing of **4a**, **4c**, and **4d**. Contrary to this, 9.20 and 7.91 peaks observed before thermal annealing became closer after thermal annealing and appeared at 8.20 and 8.32 for **4b**. It is essential to note that the peak intensity has increased upon thermal annealing for **4a**−**c**, which implies a higher degree of crystallinity.[43,44] However, the peak intensity of **4d** has decreased drastically upon thermal annealing, which indicates a significant change in film morphology. Usually, thermal annealing decreases the d spacing and increases the degree of crystallinity.[43,44] However, in the molecules studied here, thermal annealing has increased the degree of crystallinity and has very little impact on the d spacing. This inference implies that the film morphology is an important aspect, which must be studied and then correlated with the device metrics.

White light interferometry based surface profiling (WLISP) provides valuable information about the surface texture of thin films over a large area (mm^2).[45,46] Quantitative information on the three-dimensional topography of surfaces are obtained by the interference pattern of light waves with the surfaces.[47] For these experiments, SiO_2 substrates were used (similar substrates were used for OFET device fabrication) to avoid discrepancies emanating from the nature of substrate surface. The substrates were coated with the small molecules (**4a**−**d**), and surface roughness was determined for unannealed and annealed small molecule film surfaces. The average roughness factor (R_a) was lowest for **4a** (1.0) and highest for **4d** (1.4), while unannealed films were subjected to WLISP.

The increased roughness is the likely reason for drastically decreased μ for **4d**. Thermal annealing did not vary the R_a, except for **4d**. The R_a decreased by 50% for **4d**, which is likely due to the smoothening of the films upon melting at 150 °C. Atomic force microscopy (AFM) is a useful tool to monitor the thin film morphology;[48−50] hence it was used to study the morphology of thin films of **4a**−**d** prepared on hexamethyldisilazane coated SiO_2 substrates. Compounds **4a** and **4b** showed a film with crests and troughs, which changed to large agglomerates upon thermal annealing (Figure 4a and b). It is essential to note that the agglomerate formation did not disrupt the continuity of the film. On the other hand, a globular morphology was observed for **4c** that transformed to rod shape morphology upon thermal annealing at 150 °C (Figure 4c and d). However, it is necessary to note that the aspect ratio of the nanorods is low. The change in morphology has been attributed to the interaction between alkyl chains of the modified substrates and the small molecules.[51,52] In case of **4d**, there was no significant change in the film morphology upon thermal annealing as observed by AFM imaging. However, it should be noted that AFM studies are not reliable in films with increased roughness.

After the molecular characterization, we prepared field effect transistors using prefabricated bottom gate (SiO_2) and bottom contact (Au) silicon wafer substrates.[13,53] The channel width and length were 10 mm and 10 μ, respectively. Compounds **4a−d** were spun on top of the hexamethylenedisilazane modified substrates,[54−56] and the device characterization was carried out under atmospheric conditions. The drain voltage (V_D) was varied between 0 and −90 V while holding constant negative gate voltages (V_G). The output characteristics of **4a−c** showed well-defined linear and saturation regimes, indicating that **4a−c** are hole transporters. A representative output characteristic curve is shown in Figure 5a. Contrary to this, immeasurably small and noisy drain currents were observed in the case of **4d**. The transfer characteristics curves were obtained by sweeping the V_G and holding the V_D at −90 V (determined from the output characteristics; Figure 5b). The charge carrier mobility (μ) in the saturation regime was calculated using the following relationship $I_D = (\mu CW/2L)[(V_G - V_T)^2]$. The OFET parameters for **4a−c** are summarized in Table 1. The charge carrier mobility (μ) of **4c** was calculated to be three orders higher than that of its lower alkyl chain analogs (**4a** and **4b**). The high μ of 0.3 $cm^2/(V\ s)$ measured for **4c** without thermal annealing is an indication of its suitability to coat on flexible substrates, which are unstable to thermal treatments. In order to study the impact of thermal annealing, the devices were annealed at 150 °C under an argon atmosphere for 10 min. Please note that this temperature is above T_g; hence the small molecule chains were allowed to move and reach a thermodynamically stable state. Thermal annealing was found to increase the μ of **4a** and **4b** to 1×10^{-3} $cm^2/(V\ s)$. The μ of **4c** increased from 0.3 to 0.5 $cm^2/(V\ s)$. This result indicates that the thermal annealing did not have a significant impact on the efficiency of the devices fabricated using **4c**. It is necessary to note that the charge carrier mobility of TPA-*i*Ind-TPA did not vary linearly as a function of increase in the number of carbons in the alkyl chain. Indeed, we observed a drastic decrease in μ while going from octyl chain (**4c**) to decyl chain (**4d**) substituted TPA-*i*Ind-TPA. A similar trend was observed in case of poly(3-alkyl thiophene), which has been attributed to variations in thin film morphology including roughness and grain boundaries.[57] Recently, device efficiency has been found to vary nonlinearly as a function of alkyl chain length, which has been attributed to the change in self-assembly, which impacted the nanostructural order and morphology of the conjugated polymer.[39] In fact, in the small molecules studied in this work, the interplanar spacing (d) did not change upon thermal annealing, but a change in morphology was observed by AFM and WLISP. Thus, the moderate increase in charge carrier mobility as a function of thermal annealing is attributed to a change in morphology. The threshold voltage (V_T) and I_{on}/I_{off} has been found to be high, which has been the characteristic of *i*Ind based materials.[58]

3. CONCLUSION

In conclusion, we have synthesized small molecules with *i*Ind as an acceptor and TPA as a donor. The oligomer with alternate donors and acceptors exhibits a lower band gap than its individual components (1.8 eV). The quadrupole−quadrupole interaction arising from the *i*Ind and the presence of an octyl chain in the small molecules improved the interchain contacts, which in turn enhanced the hole carrier mobility. We have demonstrated that the increased intermolecular contacts leads to a material with hole carrier mobility as high as 0.3 $cm^2/(V\ s)$ without thermal annealing. This hole carrier mobility was increased to 0.5 $cm^2/(V\ s)$ upon thermal annealing. It is essential to note that the intermolecular spacing did not vary as function of time; hence the moderate increase in hole carrier mobility has been attributed to a change in thin film morphology. This approach opens up the possibility of connecting π stacking electron donors with *i*Ind to further improve the device efficiencies.

4. EXPERIMENTAL SECTION

Synthesis Procedure for Compound 1. To the suspension of 6-bromooxindole (1 g, 4.7 mmol) and 6-bromoisatin (1.06 g, 4.7 mmol) in acetic acid (30 mL), conc. HCl solution (0.2 mL) was added and heated at 100 °C for 24 h. The mixture was allowed to cool and was filtered. The solid was washed with ethyl acetate, ethanol, and water; after drying in a vacuum, it gives brown powder 6,6′-dibromoisoindigo (1.8 g, 91%).

Synthesis Procedure for Compound 2. To the solution of 6,6-dibromoisoindigo (1.7 g, 4.0 mmol) and potassium carbonate (1.38 g, 10 mmol) in N,N-dimethylformamide (DMF; 50 mL), octyl bromide (1.8 g, 9.3 mmol) was added under an argon atmosphere. The mixture was heated at 110 °C for 15 h, and the solvent was removed under reduced pressure. And the solid was dissolved in chloroform and washed with water (3 × 50 mL). The combined organic layer was washed with brine solution and dried over (Na_2SO_4) and concentrated under reduced pressure. The residue was purified using silica gel chromatography with eluting (petroleum ether (PE): DCM) to afford **2c** as deep red solid (2.1g, 81%).

Synthesis Procedure for Compound 3. 6,6′-(N,N′-dioctyl)-dibromoisoindigo (1.5 g, 2.9 mmol), bis(pinacolato) diboron (1.62 g, 6.4 mmol), [$PdCl_2$(dppf)] (80 mg), and potassium acetate (1.7 g, 17 mmol) were mixed at room temperature under an argon atmosphere. Anhydrous 1,4-dioxane (15 mL) was added through a septum. The solution was heated at 80 °C for 30 h and then cooled to room temperature. The reaction mixture was filtered through short pad silica gel, washed with methylene chloride. The collected filtration was concentrated and precipitated in cold methanol (30 mL). The precipitates were filtered and dried to give **3c** as a dark red powder (1.3 g, 76%).

Synthesis Procedure for Compound 4a−d. In a flame-dried two neck round-bottom flask (50 mL), N,N′-dialkyl-6,6′-bis(4,4,5,5-tetramethyl-1,3,2-dioxaborolan-2-yl)isoindigo (0.5 g, 0.67 mmol), 4-bromotriphenylamine (0.47 g, 1.42 mmol), and $Pd(PPh_3)_4$(0.2 g) were added. The flask was evacuated and backfilled with argon three times. Degassed toluene (30 mL) and ethanol (15 mL) and Cs_2CO_3 in water (15 m L, 2.3 mmol) were added to the flask through a septum, and the resulting solution was refluxed at 110 °C for 48 h. After cooling, the resulting solution was extracted with CH_2Cl_2 (3 × 20 mL). The organic layer was washed with brine solution and water and dried over Na_2SO_4. The solvent was removed under reduced pressure, and a purple solid was purified by column chromatography, eluting with ethyl acetate/pet. ether (8.5:1.5) to give a dark blue solid.

Compound ***4a***. Yield: 0.2 g, 30%. ^{1}H NMR (400 MHz, $CDCl_3$): δ 9.22 (d, J = 8.44 Hz, 2H), 7.53 (d, J = 8.44 Hz, 4H), 7.30−7.25 (m, 10H), 7.15−7.08 (m, 16H), 7.05 (s, 2H), 3.83 (t, J = 7.11 Hz, 4H), 1.73 (m, 4H), 1.45 (m, 4H), 0.97 (t, J = 7.37 Hz, 6H). ^{13}C NMR (100 MHz, $CDCl_3$): δ 168.45, 148.11, 147.41, 145.30, 144.42, 132.13, 130.21, 129.36, 127.73, 124.80, 123.37, 123.18, 120.56, 120.19, 105.68, 39.82, 29.73, 20.33, 13.81. MALDI-TOF (m/z): 862.1072 $(M + H)^+$.

Compound ***4b***. Yield: 0.2 g, 30%. ^{1}H NMR (400 MHz, $CDCl_3$): δ 9.22 (d, J = 8.46, 2H), 7.53 (d, J = 8.65 Hz, 4H), 7.30−7.25 (m,10H), 7.15−7.08 (m, 16H), 7.05 (s,2H), 3.82 (t, J = 7.35 Hz, 4H), 1.71 (m, 4H), 1.33 (m, 12H), 0.81 (t, J = 6.97 Hz, 6H). ^{13}C NMR (100 MHz, $CDCl_3$): δ −168.45, 148.12, 147.42, 145.30, 144.46, 133.96, 132.18, 129.40, 128.93, 127.78, 127.14, 124.80, 123.38, 120.56, 120.22, 106.45, 105.73, 40.11, 31.57, 29.71, 27.69, 26.79, 22.52, 13.56. MALDI-TOF (m/z): 917.83 $(M + H)^+$.

Compound ***4c***. Yield: 0.22 g, 37%. ^{1}H NMR (400 MHz, $CDCl_3$): δ 9.22 (d, J = 8.4 Hz, 2H), 7.53 (d, J = 8.72 Hz, 4H), 7.30−7.25 (m,

10H), 7.15−7.08 (m, 16H), 7.05 (s, 2H), 3.82 (t, J = 7.26 Hz, 4H), 1.73 (m, 4H), 1.41 (m, 4H), 1.25 (m, 16H), 0.84 (t, J = 6.67 Hz, 6H). ^{13}C NMR (100 MHz, $CDCl_3$): δ −167.78, 147.47, 146.76, 144.66, 143.78, 133.30, 129.56, 128.73, 127.10, 124.16, 122.72, 122.54, 119.91, 119.55, 105.05, 61.80, 39.43, 31.14, 28.54, 26.44, 21.97, 13.42. MALDI-TOF (m/z): 974.19 $(M + H)^+$.

Compound ***4d***. Yield: 0.21 g, 36%. ^{1}H NMR (400 MHz, $CDCl_3$): δ 9.22 (d, J = 8.52 Hz, 2H), 7.53 (d, J = 8.52 Hz, 4H), 7.30−7.25 (m, 10H), 7.15−7.08 (m, 16H), 7.05 (s, 2H), 3.82 (t, J = 7.31 Hz, 4H), 1.73 (m, 4H), 1.41 (m, 4H), 1.24 (m, 24H), 0.86 (t, J = 6.48 Hz, 6H). ^{13}C NMR (100 MHz, $CDCl_3$): δ - 168.09, 147.76, 147.05, 144.95, 144.09, 132.00, 129.83, 129.20, 129.04, 127.57,127.42,125.40, 124.45, 123.03, 122.84, 120.19, 119.86, 105.37, 39.75, 31.52, 29.37, 29.20,29.03, 28.95, 27.30, 26.75, 22.32, 13.78. MALDI-TOF (m/z): 1030.88 $(M + H)^+$.

■ ASSOCIATED CONTENT

Ⓢ Supporting Information

Synthetic procedures, cyclic voltammograms, thermograms, surface plots, and IV curves are available. This material is available free of charge via the Internet at http://pubs.acs.org.

■ AUTHOR INFORMATION

Corresponding Author

*Tel: +91-20-25903075. E-mail: k.krishnamoorthy@ncl.res.in.

Author Contributions

The manuscript was written through contributions of all authors. All authors have given approval to the final version of the manuscript.

Notes

The authors declare no competing financial interest.

■ ACKNOWLEDGMENTS

We thank Dr. J. Nithyanandhan and Dr. Kumar Vanka for valuable discussions. The funding from CSIR is greatly acknowledged (TAPSUN NWP 0054). S.S.D. and A.A. thank CSIR-India for scholarship. CD acknowledges scholarship from UGC-India.

■ REFERENCES

(1) Facchetti, A. *Chem. Mater.* **2011**, *23*, 733−758.
(2) Zhao, X.; Zhan, X. *Chem. Soc. Rev.* **2011**, *40*, 3728−3743.
(3) Biniek, L.; Schroeder, B. C.; Nielsen, C. B.; McCulloch, I. *J. Mater. Chem.* **2012**, *22*, 14803−14813.
(4) Zaumseil, J.; Sirringhaus, H. *Chem. Rev.* **2007**, *107*, 1296−1323.
(5) Kanimozhi, C.; Yaacobi-Gross, N.; Chou, K. W.; Amassian, A.; Anthopoulos, T. D.; Patil, S. *J. Am. Chem. Soc.* **2012**, *134*, 16532−16535.
(6) Huang, F.; Chen, K.-S.; Yip, H.-L.; Hau, S. K.; Acton, O.; Zhang, Y.; Luo, J. D.; Jen, A. K.-Y. *J. Am. Chem. Soc.* **2009**, *131*, 13886−13887.
(7) Murphy, A. R.; Fréchet, J. M. J. *Chem. Rev.* **2007**, *107*, 1066−1096.
(8) Singh, K.; Singh Virk, T.; Zhang, J.; Xu, W.; Zhu, D. *Chem. Commun.* **2012**, *48*, 12174−12176.
(9) Li, Y.; Guo, Q.; Li, Z.; Pei, J.; Tian, W. *Energy Environ. Sci.* **2010**, *3*, 1427−1436.
(10) Kang, J.; Shin, N.; Jang, D. Y.; Prabhu, V. M.; Yoon, D. Y. *J. Am. Chem. Soc.* **2008**, *130*, 12273−12275.
(11) Zhong, H.; Smith, J.; Rossbauer, S.; White, A. J. P.; Anthopoulos, T. D.; Heeney, M. *Adv. Mater.* **2012**, *24*, 3205−3211.
(12) Qiao, Y.; Guo, Y.; Yu, C.; Zhang, F.; Xu, W.; Liu, Y.; Zhu, D. *J. Am. Chem. Soc.* **2012**, *134*, 4084−4087.
(13) Arulkashmir, A.; Mahale, R. Y.; Dharmapurikar, S. S.; Jangid, M. K.; Krishnamoorthy, K. *Polym. Chem.* **2012**, *3*, 1641−1646.
(14) Lee, O. P.; Yiu, A. T.; Beaujuge, P. M.; Woo, C. H.; Holcombe, T. W.; Millstone, J. E.; Douglas, J. D.; Chen, M. S.; Fréchet, J. M. J. *Adv. Mater.* **2011**, *23*, 5359−5363.
(15) Kanibolotsky, A. L.; Vilela, F.; Forgie, J. C.; Elmasly, S. E. T.; Skabara, P. J.; Zhang, K.; Tieke, B.; McGurk, J.; Belton, C. R.; Stavrinou, P. N.; Bradley, D. D. C. *Adv. Mater.* **2011**, *23*, 2093−2097.
(16) Yassin, A.; Leriche, P.; Allain, M.; Roncali, J. *New J. Chem.* **2013**, *37*, 502−507.
(17) Zhang, M.; Tsao, H. N.; Pisula, W.; Yang, C.; Mishra, A. K.; Müllen, K. *J. Am. Chem. Soc.* **2007**, *129*, 3472−3473.
(18) Popere, B. C.; Della Pelle, A. M.; Thayumanavan, S. *Macromolecules* **2011**, *44*, 4767−4776.
(19) Cai, Z.; Guo, Y.; Yang, S.; Peng, Q.; Luo, H.; Liu, Z.; Zhang, G.; Liu, Y.; Zhang, D. *Chem. Mater.* **2013**, *25*, 471−478.
(20) Xue, L.; He, J.; Gu, X.; Yang, Z.; Xu, B.; Tian, W. *J. Phys. Chem. C* **2009**, *113*, 12911−12917.
(21) Steckler, T. T.; Zhang, X.; Hwang, J.; Honeyager, R.; Ohira, S.; Zhang, X.-H.; Grant, A.; Ellinger, S.; Odom, S. A.; Sweat, D. A. *J. Am. Chem. Soc.* **2009**, *131*, 2824−2826.
(22) Polander, L. E.; Pandey, L.; Barlow, S.; Tiwari, S. P.; Risko, C.; Kippelen, B.; Bredas, J.-L.; Marder, S. R. *J. Phys. Chem. C* **2011**, *115*, 23149−23163.
(23) Cortizo-Lacalle, D.; Arumugam, S.; Elmasly, S. E. T.; Kanibolotsky, A. L.; Findlay, N. J.; Inigo, A. R.; Skabara, P. J. *J. Mater. Chem.* **2012**, *22*, 11310−11315.
(24) Bedi, A.; Senanayak, S. P.; Das, S.; Narayan, K. S.; Zade, S. S. *Polym. Chem.* **2012**, *3*, 1453−1460.
(25) Chen, Z.; Lee, M. J.; Ashraf, R. S.; Gu, Y.; Albert-Seifried, S.; Nielsen, M. M.; Schroeder, B.; Anthopoulos, T. D.; Heeney, M.; McCulloch, I.; Sirringhaus, H. *Adv. Mater.* **2012**, *24*, 647−652.
(26) Lei, T.; Cao, Y.; Zhou, X.; Peng, Y.; Bian, J.; Pei, J. *Chem. Mater.* **2012**, *24*, 1762−1770.
(27) Mei, J.; Kim, D. H.; Ayzner, A. L.; Toney, M. F.; Bao, Z. *J. Am. Chem. Soc.* **2011**, *133*, 20130−20133.
(28) Sonar, P.; Tan, H.-S.; Sun, S.; Lam, Y. M.; Dodabalapur, A. *Polym. Chem.* **2013**, *4*, 1983−1994.
(29) Hou, Q.; Chen, Y.; Zhen, H.; Ma, Z.; Hong, W.; Shi, G.; Zhang, F. *J. Mater. Chem. A* **2013**, *1*, 4937−4940.
(30) Sonntag, M.; Kreger, K.; Hanft, D.; Strohriegl, P.; Setayesh, S.; de Leeuw, D. *Chem. Mater.* **2005**, *17*, 3031−3039.
(31) Roquet, S.; Cravino, A.; Leriche, P.; Alévêque, O.; Frère, P.; Roncali, J. *J. Am. Chem. Soc.* **2006**, *128*, 3459−3466.
(32) Piliego, C.; Holcombe, T. W.; Douglas, J. D.; Woo, C. H.; Beaujuge, P. M.; Fréchet, J. M. J. *J. Am. Chem. Soc.* **2010**, *132*, 7595−7597.
(33) Zoombelt, A. P.; Leenen, M. A. M.; Fonrodona, M.; Nicolas, Y.; Wienk, M. M.; Janssen, R. A. J. *Polymer* **2009**, *50*, 4564−4570.
(34) Osaka, I.; Zhang, R.; Sauvé, G.; Smilgies, D.-M.; Kowalewski, T.; McCullough, R. D. *J. Am. Chem. Soc.* **2009**, *131*, 2521−2529.
(35) Zhang, L.; Colella, N. S.; Liu, F.; Trahan, S.; Baral, J. K.; Winter, H. H.; Mannsfeld, S. C. B.; Briseno, A. L. *J. Am. Chem. Soc.* **2013**, *135*, 844−854.
(36) Fitzner, R.; Elschner, C.; Weil, M.; Uhrich, C.; Körner, C.; Riede, M.; Leo, K.; Pfeiffer, M.; Reinold, E.; Mena-Osteritz, E.; Bäuerle, P. *Adv. Mater.* **2012**, *24*, 675−680.
(37) Izawa, T.; Miyazaki, E.; Takimiya, K. *Adv. Mater.* **2008**, *20*, 3388−3392.
(38) Minari, T.; Miyata, Y.; Terayama, M.; Nemoto, T.; Nishinaga, T.; Komatsu, K.; Isoda, S. *Appl. Phys. Lett.* **2006**, *88*, 083514/1−083514/3.
(39) Cabanetos, C.; Labban, A. E.; Bartelt, J. A.; Douglas, J. D.; Mateker, W. R.; Fréchet, J. M. J.; McGehee, M. D.; Beaujuge, P. M. *J. Am. Chem. Soc.* **2013**, *135*, 4656−4659.
(40) Stalder, R.; Mei, J.; Subbiah, J.; Grand, C.; Estrada, L. A.; So, F.; Reynolds, J. R. *Macromolecules* **2011**, *44*, 6303−6310.
(41) Mei, J.; Graham, K. R.; Stalder, R.; Reynolds, J. R. *Org. Lett.* **2010**, *12*, 660−663.
(42) Thompson, B. C.; Kim, Y.-G.; Reynolds, J. R. *Macromolecules* **2005**, *38*, 5359−5362.

(43) Tantiwiwat, M.; Tamayo, A.; Luu, N.; Dang, X.-D.; Nguyen, T.-Q. *J. Phys. Chem. C* **2008**, *112*, 17402−17407.
(44) Kim, Y.-H.; Lee, Y. U.; Han, J.-I.; Han, S.-M.; Han, M.-K. *J. Electrochem. Soc.* **2007**, *154*, H995−H998.
(45) Diethert, A.; Körstgens, V.; Magerl, D.; Ecker, K.; Perlich, J.; Roth, S. V.; Müller-Buschbaum, P. *ACS Appl. Mater. Interfaces* **2012**, *4*, 3951−3958.
(46) Aulin, C.; Ström, G. *Ind. Eng. Chem. Res.* **2013**, *52*, 2582−2589.
(47) Yilgor, I.; Bilgin, S.; Isik, M.; Yilgor, E. *Langmuir* **2012**, *28*, 14808−14814.
(48) Sun, Y.; Chien, S.-C.; Yip, H.-L.; Chen, K.-S.; Zhang, Y.; Davies, J. A.; Chen, F.-C.; Lin, B.; Jen, A. K.-Y. *J. Mater. Chem.* **2012**, *22*, 5587−5595.
(49) Durban, M. M.; Kazarinoff, P. D.; Luscombe, C. K. *Macromolecules* **2010**, *43*, 6348−6352.
(50) Kim, J.-H.; Song, C. E.; Kang, I.-N.; Shin, W. S.; Hwang, D.-H. *Chem. Commun.* **2013**, *49*, 3248−3250.
(51) Bock, C.; Pham, D. V.; Kunze, U.; Käfer, D.; Witte, G.; Wöll, C. *J. Appl. Phys.* **2006**, *100*, 114517−1−114517−7.
(52) Tsao, H. N.; Pisula, W.; Liu, Z.; Osikowicz, W.; Salaneck, W. R.; Müllen, K. *Adv. Mater.* **2008**, *20*, 2715−2719.
(53) Izuhara, D.; Swager, T. M. *J. Am. Chem. Soc.* **2009**, *131*, 17724−17725.
(54) Park, S. H.; Lee, H. S.; Kim, J.-D.; Breiby, D. W.; Kim, E.; Park, Y. D.; Ryu, D. Y.; Lee, D. R.; Cho, J. H. *J. Mater. Chem.* **2011**, *21*, 15580−15586.
(55) Hüttner, S.; Sommer, M.; Thelakkat, M. *Appl. Phys. Lett.* **2008**, *92*, 093302/1−093302/3.
(56) Ortiz, R. P.; Facchetti, A.; Marks, T. J. *Chem. Rev.* **2010**, *110*, 205−239.
(57) Babel, A.; Jenekhe, S. A. *Synth. Met.* **2005**, *148*, 169−173.
(58) Lei, T.; Dou, J.-H.; Ma, Z.-J.; Yao, C.-H.; Liu, C.-J.; Wang, J.-Y.; Pei, J. *J. Am. Chem. Soc.* **2012**, *134*, 20025−20028.